Mutations in the PX−$SH3_A$ Linker of $p47^{phox}$ Decouple $PI(3,4)P_2$ Binding from NADPH Oxidase Activation†

Kai Shen, Susan Sergeant, Roy R. Hantgan, Linda C. McPhail, and David A. Horita*

Department of Biochemistry, Wake Forest University School of Medicine, Medical Center Boulevard, Winston-Salem, North Carolina 27157-1016

Received April 3, 2008; Revised Manuscript Received June 19, 2008

ABSTRACT: NADPH oxidase is essential in the human innate immune response. $p47^{phox}$, a cytosolic NADPH oxidase component, plays a regulatory role in the activation of NADPH oxidase. Our manipulation of $p47^{phox}$ by mutation and amino acid deletion shows that the linker region between the PX and N-terminal SH3 domain plays a role in blocking the binding of the phosphoinositide 3,4-bisphosphate [$PI(3,4)P_2$], a lipid second messenger generated upon neutrophil activation. Replacement of linker residues 151−158 with glycine alters NMR-measured spin lattice relaxation rates and sedimentation velocity compared to those of the wild-type protein, suggesting that the PX domain is released from its autoinhibited conformation. Liposome binding and surface plasmon resonance experiments confirm this result, showing that this mutant has a similar binding affinity for the isolated PX domain toward $PI(3,4)P_2$. However, an in vitro NADPH oxidase activity assay reveals that this glycine mutant of the full-length protein greatly reduced NADPH oxidase activity upon activation even though it displayed $PI(3,4)P_2$ binding activity comparable to that of the isolated PX domain. Our results highlight an active role of the PX−SH3 linker region in maintaining $p47^{phox}$ in its fully autoinhibited form and demonstrate that binding of $p47^{phox}$ to membrane phospholipids is mechanistically distinct from NADPH oxidase activation.

Neutrophils play a central role in the immune response (*1*). The reactive oxygen species (ROS)[1] generated by activated NADPH oxidase in neutrophils and macrophages are used by the host to kill invading microorganisms (*2, 3*). The importance of NADPH oxidase in host defense has been demonstrated to play crucial roles during the oxidase activation as evidenced by chronic granulomatous disease (CGD) patients, who suffer from repeated infections due to a lack of ROS generation capability during infection because of NADPH oxidase mutations (*4*). ROS also play crucial roles in signal transduction pathways. Recent studies of the nonphagocytic NADPH oxidases reveal that ROS regulate signal transduction in a series of cell events involved in a variety of diseases (*3, 5*). The production of ROS should thus be tightly regulated as both over- and underproduction are detrimental to proper cellular function.

Phagocytic NADPH oxidase is composed of six individual proteins (*6*). Two are integral membrane proteins: $gp91^{phox}$ and $p22^{phox}$. The other four proteins ($p47^{phox}$, $p67^{phox}$, $p40^{phox}$, and a small G protein Rac) are localized in the resting cell cytosol. These four proteins undergo regulatory changes during the activation of NADPH oxidase and have been studied in great detail over the past several decades (*2, 3, 7*). Among these four cytosolic proteins, $p47^{phox}$ is believed to act as an organizer during the assembly of NADPH oxidase (*8*). Upon cell stimulation, $p47^{phox}$ translocates other cytosolic components, i.e., $p67^{phox}$ and $p40^{phox}$, to the inner membrane, where they bind to $p22^{phox}$ and $gp91^{phox}$, along with Rac, to form a functional NADPH oxidase.

$p47^{phox}$ is composed of a Phox homology (PX) domain, tandem SH3 domains, a polybasic region/autoinhibitory region (PBR/AIR), and a proline rich region (PRR) (Figure 1A) (*7*). The current understanding of the intramolecular regulatory mechanism of $p47^{phox}$ is from both structural and functional perspectives and has been recently reviewed (*2, 9*). In unstimulated cells, $p47^{phox}$ is present in a cytosolic, autoinhibited form which has a substantially lower binding affinity for both membrane phospholipids and $p22^{phox}$. In the activated oxidase, $p47^{phox}$ is believed to bind via its PX domain to membrane phospholipids {primarily phosphatidylinositol 3,4-bisphosphate [$PI(3,4)P_2$]}, via its SH3 domains to $p22^{phox}$, and via its PRR to $p67^{phox}$ (*10*). $PI(3,4)P_2$ is a product of phosphoinositide 3-kinase in the stimulated neutrophil (*11*).

† This work was supported by Grants AI064609 (to D.A.H.) and AI022564 (to L.C.M.) from the National Institutes of Health and Grant 2006-IDG-1004 (to R.R.H.) from the North Carolina Biotechnology Center.

* To whom correspondence should be addressed. Telephone: (336) 713-4194. Fax: (336) 716-7671. E-mail: dhorita@wfubmc.edu.

[1] Abbreviations: biotin-PE, biotinylated 1-oleoyl-2-[12-biotinyl(aminododecanoyl)]-*sn*-glycero-3-phosphoethanolamine; CD, circular dichroism; CGD, chronic granulomatous disease; diC8, 1,2-dioctanoyl; egg-PC, L-α-phosphatidylcholine; egg-PE, L-α-phosphatidylethanolamine; DTT, dithiothreitol; GST, glutathione *S*-transferase; NMR, nuclear magnetic resonance; NOXO1, Nox organizing protein 1; OAG, 1-oleoyl-2-acetyl-*sn*-glycerol; OG, *n*-octyl β-D-glucopyranoside; PBR/AIR, polybasic region/autoinhibitory region; $PI(3,4)P_2$, phosphoinositide 3,4-bisphosphate; POPC, 1-palmitoyl-2-oleoyl-*sn*-glycero-3-phosphocholine; POPE, 1-palmitoyl-2-oleoyl-*sn*-glycero-3-phosphoethanolamine; PRR, proline rich region; PX, Phox homology; ROS, reactive oxygen species; SOD, superoxide dismutase; R_1, spin lattice relaxation rate; RU, response unit; SAXS, small-angle X-ray scattering spectroscopy; $SH3_A$, N-terminal SH3; $SH3_B$, C-terminal SH3; SPR, surface plasmon resonance.

10.1021/bi8005847 CCC: $40.75
Published on Web 08/02/2008

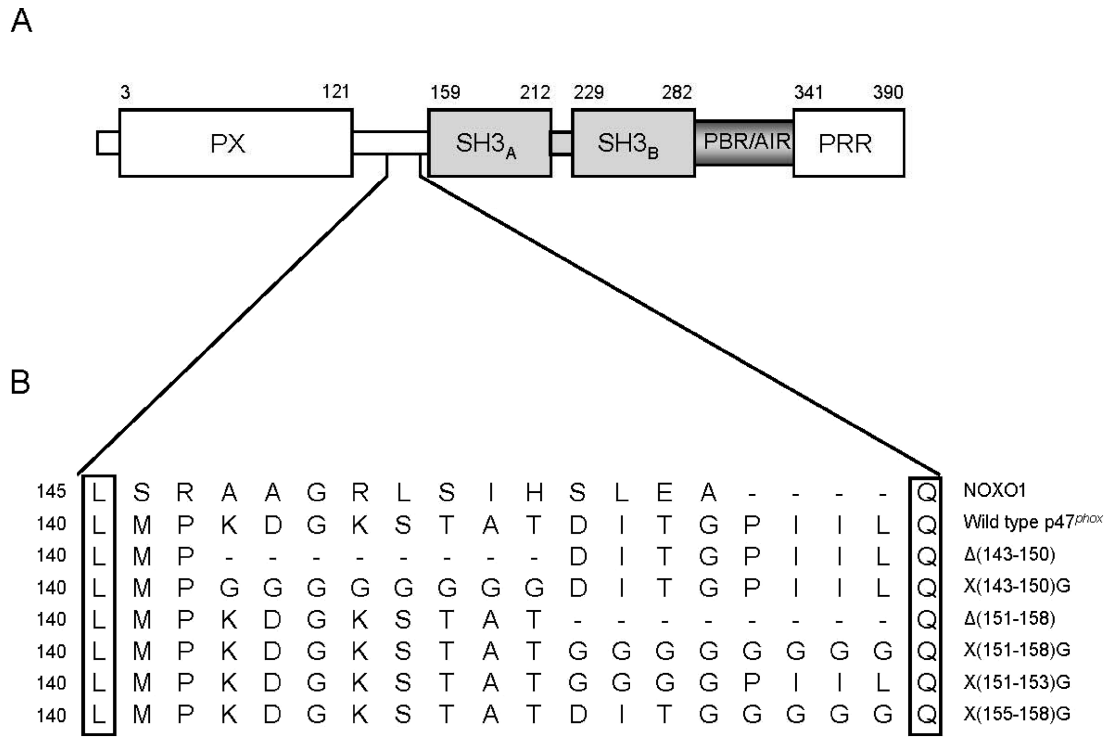

FIGURE 1: p47*phox* domain arrangement (A) and alignment of NOXO1, wild-type p47*phox*, and mutants prepared in this study (B). The NOXO1 sequence was retrieved from SWISS-Prot entry Q8NFA2.

Crystallographic and nuclear magnetic resonance (NMR) spectroscopic studies of p47*phox* show that the tandem SH3 domains, the binding target of the p22*phox* C-terminal polyproline region, are blocked by the PBR/AIR in the autoinhibited form and that phosphorylation of the PBR/AIR eliminates this intramolecular interaction and allows binding between the p47*phox* SH3 domains and the p22*phox* C-terminal tail (*12, 13*). The interaction between the PX domain and $PI(3,4)P_2$ is also masked by intramolecular interactions (*14, 15*). There are, however, conflicting hypotheses about the specific nature of this autoinhibitory interaction. There are two principle models defining the intramolecular interactions between the PX domain and the remainder of p47*phox*.

One model suggests that the PxxP motif in the PX domain interacts with the C-terminal SH3 domain ($SH3_B$), impeding $PI(3,4)P_2$ binding (*14–16*). The W263R mutation in $SH3_B$ strengthens binding between the PX domain and $PI(3,4)P_2$, implying that the PX domain is released after the intramolecular interaction between these two domains is broken (*14, 15*). More recently, a different domain arrangement model was put forth by Durand et al. (*17*) based on their study of full-length p47*phox* in solution using small-angle X-ray scattering spectroscopy (SAXS). They suggested that full-length p47*phox* in solution assumes an extended conformation, even in the autoinhibited form, and that the PX domain in autoinhibited p47*phox* may directly interact with the PBR/AIR instead of the $SH3_B$ domain and therefore prevent p47*phox* from binding to $PI(3,4)P_2$ and p22*phox*. Although both models have supporting data, neither can successfully explain all published biochemical data to date. The first model is inconsistent with the crystal structure of the autoinhibited tandem SH3 domains (*12*), which spans residues ~156−340 and includes the tandem SH3 domains and the PBR/AIR. These structures show that both SH3 domains are required to form the PBR/AIR binding interface and that W263 in $SH3_B$ is not available to interact directly with the PX domain (*12, 13, 18*). In contrast, the SAXS-derived model of Durand et al. (*17*) does not explain why the W263R mutant leads to enhanced $PI(3,4)P_2$ binding.

Specific interactions between the PX domain and the phosphoinositides in membranes are believed to dictate translocation of p47*phox* and p40*phox* to the membrane and play significant physiological roles in NADPH oxidase activation (*16, 19, 20*). A more detailed understanding of the mechanism by which the p47*phox* PX domain is released from the autoinhibited form is thus crucial to a complete understanding of NADPH oxidase activation. Structural analysis of the PX−$SH3_A$ linker region by SAXS and sequence analysis yielded inconclusive results, indicating that this region does not adopt canonical secondary structural elements but is also not completely disordered (*17*). Portions of the linker, however, are required for association of p47*phox* with p22*phox* during translocation (*21, 22*). Currently, there are no direct studies addressing the structural basis of the linker region's contribution to the autoinhibited p47*phox*. Inspired by the coupling model between SH2 and SH3 domains in Src kinase in which the linker region between the domains forms a "snap-lock" that locks the relative orientation of these two domains together (*23*), we have investigated the role of the PX−$SH3_A$ linker region with a combination of biophysical analyses and mutagenesis. Our findings show that the linker region between residues 151 and 158 is involved in intramolecular inhibition of binding of the PX domain to $PI(3,4)P_2$. Our data indicate that the PX domain is released for $PI(3,4)P_2$ binding by either removal of residues 151−158 or mutation of them to glycines. Surprisingly, release of the PX domain hinders activation of NADPH oxidase, which gives a new view on the relationship between PX and the remainder of p47*phox*.

EXPERIMENTAL PROCEDURES

Protein Preparation. cDNAs of human $p47^{phox}$ and Rac1 (Q61L) were generous gifts from T. Leto of the National Institutes of Health (Bethesda, MD). $p67^{phox}$ plasmid was kindly provided by D. Lambeth of Emory University (Atlanta, GA). Mutants of human $p47^{phox}$ were prepared with the Quickchange site-directed mutagenesis kit (Stratagene, La Jolla, CA) with appropriate primers (Operon, Huntsville, AL). All constructs, including $p47^{phox}$, $p67^{phox}$, and Rac1 (Q61L), were verified by DNA sequencing at an in-house DNA sequencing facility. cDNAs were then cloned into the pGEX-6P-1 vector (GE Healthcare, Uppsala, Sweden) and expressed in *Escherichia coli* BL21. Cells were grown in M9 minimal medium with 100 μg/mL ampicillin at 37 °C. Protein expression was induced by first cooling the cell culture to 15 °C at an OD_{600} approaching 0.6 and adding isopropyl β-D-1-thiogalactopyranoside (IPTG) to a final concentration of 0.5 mM. Cells were then grown at 15 °C overnight (48−72 h for cells grown in D_2O) and harvested by centrifugation (4000*g* for 30 min). Full-length (residues 1−390) and C-terminally truncated (residues 1−340) ^{15}N-labeled proteins were grown with 1 g of $^{15}NH_4Cl$ (Cambridge Isotope Laboratory, Andover, MA) per liter of medium as the sole nitrogen source. ^{15}N relaxation data were acquired on $p47^{phox}$ constructs spanning residues 1−340. ^{2}H-, ^{13}C-, and ^{15}N-labeled proteins for NMR relaxation studies were grown utilizing 1 g of $^{15}NH_4Cl$ and 2 g of [^{2}H,^{13}C]glucose (Cambridge Isotope Laboratory) per liter of 99% D_2O (Spectra Stable Isotope, Columbia, MD) medium.

Cell pellets were resuspended in a lysis buffer [20 mM NaCl, 20 mM Tris-HCl, and 2 mM dithiothreitol (DTT) (pH 7.5)], and cells were lysed by sonication. Cell lysate of 1 L of cell growth was treated with 10 μL of 25 units/μL Benzonase nuclease (Novagen, Madison, WI) and centrifuged (15000*g* for 30 min). Supernatant-containing soluble GST-tagged fusion proteins were captured with glutathione Sepharose FF resin (GE Healthcare), eluted, and digested with Precision Protease (GE Healthcare) to remove the glutathione *S*-transferase (GST) tag. The cleaved products were loaded on a SP-Sepharose ion exchange column (GE Healthcare) to separate the GST tag and desired proteins. All proteins were concentrated in a Vivaspin 15R 10 kDa concentrator (Sartorius, Goettingen, Germany) with an appropriate buffer. The purity and protein size were examined on a Superdex size exclusion column (GE Healthcare) against protein standards to ensure a pure, monomer protein for further analysis.

Liposome Preparation. Liposomes were prepared by following previous protocols (*24, 25*). $PI(3,4)P_2$(1,2-dipalmitoyl) sodium salt (Echelon, Salt Lake City, UT) was dissolved in a solvent mixture [1:2:0.8 (v/v) $CHCl_3/CH_3OH/H_2O$]. The $PI(3,4)P_2$ solution was then added to premixed L-α-phosphatidylethanolamine (egg-PE) and L-α-phosphatidylcholine (egg-PC) (Avanti, Alabaster, AL) to yield a $PI(3,4)P_2$ molar concentration of 20%. The molar ratio of egg-PE to egg-PC was kept at 4:1 (*24*). Biotinylated 1-oleoyl-2-[12-biotinyl-(aminododecanoyl)]-*sn*-glycero-3-phosphoethanolamine (0.5 mol %, biotin-PE; Avanti) was added to increase pellet efficiency. Liposomes containing 0% $PI(3,4)P_2$ were also constructed for use as controls. The mixture was then dried under a gentle N_2 flow. The dried phospholipids were subjected to high vacuum to completely remove residual chloroform. The phospholipid mixture was hydrated for 1 h with liposome binding buffer [20 mM Tris, 100 mM NaCl, and 0.1 mM DTT (pH 7.2)] and extruded 19 times with a LiposoFast extruder (Avestin, Ottawa, ON) through two stacked polycarbonate membranes (Avestin) with a pore size of 0.1 μm. The size of liposomes was examined with Zetasizer dynamic light scattering (Malvern, Worcestershire, U.K.).

Liposome Binding Assay. A previously described liposome binding assay was used (*25*). Briefly, 5 μL of 0.5 mM liposome vesicles containing 0 or 20% $PI(3,4)P_2$ was incubated with 90 μL of 0.125 μM protein in polycarbonate centrifuge tubes (Beckman, Palo Alto, CA) for 30 min at room temperature with gentle shaking. Streptavidin (5 μL of a 0.5 mg/mL solution; Sigma-Aldrich, St. Louis, MO) was added to the mixture and the mixture incubated for an additional 1 min. The tubes were then centrifuged in a Beckman TLA-120 rotor (100000*g*, 20 min, 25 °C). The supernatant was carefully removed, and the pellet was resuspended in 100 μL of liposome binding buffer. Protein contents in the supernatant and pellet were analyzed with a 12% SDS−PAGE gel. Gels were stained with blue silver stain (*26*), and protein contents in both samples were quantified with densitometry software package Alpha EaseFC (Alpha Innotech, San Leandro, CA).

Surface Plasmon Resonance (SPR) Experiments. Interactions between protein and $PI(3,4)P_2$ were investigated using SPR. Liposomes used for the SPR experiment were prepared in a manner similar to that of the liposome preparation used in the liposome binding assay except where indicated below. Synthetic 1-palmitoyl-2-oleoyl-*sn*-glycero-3-phosphocholine (POPC) and 1-palmitoyl-2-oleoyl-*sn*-glycero-3-phosphoethanolamine (POPE) (Avanti), instead of egg-PC and egg-PE, were used as "background" lipids (*27*). Liposomes were prepared with either 0 mol % $PI(3,4)P_2$ [80:20:0 POPC/POPE/$PI(3,4)P_2$] or 3 mol % $PI(3,4)P_2$ [77:20:3 POPC/POPE/$PI(3,4)P_2$]. Biotinylated PE was not included in liposomes for the SPR experiment. The SPR experiments were performed on a Biacore T100 instrument using a Biacore S series L1 sensor chip (GE Healthcare, Piscataway, NJ). The sensor channels were paired to eliminate the effects in the flow path. The reference and sample channel were assigned in such a way that the reference channel was always upstream in the flow arrangement to avoid cross contamination.

The sensor surface was first primed with running buffer [25 mM HEPES and 150 mM NaCl (pH 7.2)]. To coat the sensor surface with lipids, 0.1 mM liposomes containing either 0 or 3 mol % $PI(3,4)P_2$ were injected at a flow rate of 5 μL/min into reference or sample channels, respectively, to obtain a liposome coating level of ∼6000 response units (RU) (*27*). The use of a low initial liposome concentration coupled with a slow flow rate yielded a highly reproducible (approximately ±200 RU) lipid coating. A terminal response of 6000 RU is thought to indicate that the liposomes have spread on the surface of the sensor chip to form a bilayer (*28*). The liposome capture level was set to such a level to avoid nonspecific protein binding to the sensor surface without introducing mass transfer effects in kinetic studies (*27, 29, 30*). The captured lipsomes were washed twice with 10 μL of 50 mM NaOH at a flow rate of 100 μL/min to stabilize their surface prior to protein adsorption. Six different

concentrations of protein solution in the running buffer, ranging from 0.1 to 20 μM, were injected with a flow rate of either 5 μL/min for equilibrium or 30 μL/min for kinetic studies followed by a dissociation period in which bound protein molecules were released with a constant flow of the running buffer. We were limited to a maximum protein concentration of 20 μM because of increased solution viscosity and instrument clogging at higher protein concentrations. The lipid surface was treated with 10 μL of 50 mM NaOH at a flow rate of 100 μL/min after each protein injection to recover the baseline level prior to the next protein injection. The chip surface was regenerated with 40 mM CHAPS (Anatrace, Maumee, OH) and 40 mM *n*-octyl β-D-glucopyranoside (OG; Anatrace) to remove immobilized lipids. Sensorgrams were recorded and analyzed with both Biacore T100 evaluation software and Scrubber. Additional data analysis was performed using Sigmaplot. Equilibrium dissociation constants (K_d) were obtained from equilibrium run analyses while association rates (k_a) and dissociation rates (k_d) from kinetic run analyses. Scrubber was provided by the University of Utah's Center for Biomolecular Interaction Analysis (www.cores.utah.edu/interaction). Experiments were repeated at least three times.

Circular Dichroism (CD) Spectroscopy. CD spectra of protein samples were acquired on a Jasco J-715 CD spectrometer (JASCO, Easton, MD). Proteins were diluted in the liposome binding buffer to ~0.2 mg/mL. The absorption of the protein solution at 280 nm was recorded to calculate molar ellipticity. The CD spectrum was acquired in the range from 195 to 250 nm. For each sample, three spectra were recorded and averaged. Absorption from liposome binding buffer was subtracted from the final CD spectra.

NMR Experiments. All NMR data were acquired on a Bruker Avance DRX-600 spectrometer equipped with a triple-resonance Z-gradient Cryoprobe or a triple-resonance XYZ-gradient room-temperature probe. Prior to acquisition, proteins were concentrated to ~0.5 mM in NMR buffer [25 mM KP_i, 25 mM KCl, and 0.5 mM Na_xEDTA (pH 6.5)]. Protein concentrations were measured by the Bradford method. Maintenance of the folded conformation of the full-length and C-terminally truncated protein constructs was monitored using two-dimensional (2D) $^1H-^{15}N$ TROSY spectra (*31*). Relaxation rates (R_1) of amide ^{15}N atoms were measured for the C-terminally truncated constructs using the TROSY-HNCO scheme (*32–34*). NMR data were processed and analyzed with NMRPipe (*35*) and NMRView (*36*).

Analytical Ultracentrifugation. Proteins were prepared for analytical ultracentrifugation by dialysis against NMR buffer. Sedimentation velocity experiments were performed using a Beckman Optima XL-A analytical ultracentrifuge equipped with absorbance optics and an An60 Ti rotor. Twelve millimeter centerpiece cells were used for all samples with an initial A_{280} of ~1.0. Data were collected at 20 °C at a rotor speed of 45000 rpm over a 5 h period. Data were analyzed using both SVEDBERG version 6.39 (*37*) and DCDT+ version 2.07 (*38*) to obtain the weight-average sedimentation coefficient, S_w, and the distribution of sedimenting species, $g(s^*)$, respectively (*39–41*). $S_{20,w}$ values were calculated from sedimentation coefficients using solvent density and viscosity values from SEDNTERP version 1.09, which was obtained from http://jphilo.mailway.com/download.htm.

NADPH Oxidase Activation and Assay. Recombinant proteins ($p47^{phox}$, $p67^{phox}$, and constitutively active Rac1 Q61L) were produced in *E. coli* as described above. The membrane fraction of unstimulated neutrophils served as the source of flavocytochrome b_{558}. Human neutrophils were isolated, and membrane fractions were prepared as described previously (*42*). The flavocytochrome concentration of membranes was determined by difference spectra (γ-peak, $\varepsilon_{425} = 106\ mM^{-1}\ cm^{-1}$) (*43*). Lipid activators for the NADPH oxidase assay were freshly prepared for each assay. 1-Oleoyl-2-acetyl-*sn*-glycerol (OAG; Avanti) was prepared by sonication in water (*44*). PI(3,4)P_2-(1,2-dioctanoyl) [PI(3,4)P_2-diC8; Cell Signals, Columbus, OH] was dissolved in water, and the lipid concentration was determined by a lipid phosphorus assay (*45*). A mixture containing each lipid at 0.4 mM was prepared for addition to the NADPH oxidase assay. The semirecombinant cell-free NADPH oxidase assay was a kinetic assay modified from that of Palicz et al. (*46*). The reaction mixtures contained 50 mM Na_xPO_4 (pH 7.0), 5 mM $MgCl_2$, 1 mM EGTA, 10 μM FAD, 100 μM ferricytochrome *c*, and either 0 or 0.19 mg/mL superoxide dismutase (SOD). Recombinant NADPH oxidase proteins were present as follows: 10 pmol of $p47^{phox}$ (wild type or the indicated mutant), 5 pmol of $p67^{phox}$, and 20 pmol of Rac1 Q61L. The neutrophil membrane protein was the source of flavocytochrome b_{558} (2.55 pmol). After the addition of 100 μM PI(3,4)P_2-diC_8 and OAG each or water (final volume, 120 μL), the reaction mixture was incubated for 90 min at 25 °C. At the end of the incubation time, paired reaction mixtures (with or without SOD) were transferred to spectrophotometric cuvettes containing NADPH (final concentration, 200 μM). The change in absorbance at 550 nm was recorded (Shimadzu, UV-2401 PC) for 1 min, with the SOD-containing cuvette as the reference. The slope of the line was used to calculate the rate of cytochrome *c* reduction ($\varepsilon_{550} = 21\ mM^{-1}\ cm^{-1}$) (*47*). Activity is expressed as nanomoles of O_2^- per minute per picomole of flavocytochrome b_{558}. Triplicate determinations were performed for each $p47^{phox}$−activator combination.

RESULTS

Mutations in the PX−$SH3_A$ Linker Region Do Not Disrupt Individual Domain Structures. Because point mutations can disrupt global protein structure, we sought to verify that the PX and SH3 domain structures were not affected by mutations to the linker region. The various mutation and deletion constructs in the linker region are compiled in Figure 1B. On the basis of the X-ray structures of the PX domain [PDB entry 1KQ6 (unpublished)] in which the final β-strand extends through residue 140 and of the tandem SH3/PBR [PDB entry 1NG2 (*12*)] in which the first β-strand begins at residue 160, we chose to mutate two consecutive regions in the PX−$SH3_A$ linker, residues 143−150 and 151−158. We have analyzed constructs with these residues deleted and with these residues replaced with glycines. Unlike the deletion constructs, which have a shorter linker, the glycine mutation preserves the linker length while rendering that span less likely to form stable secondary structure elements (*23*). Nox

organizing protein 1 (NOXO1) β1, a p47^{phox} PX homologue involved in nonphagocytic NADPH oxidases, was reported to have constitutive binding to phosphatidylinositols (*48, 49*). Notably, the linker region between the PX and neighbor SH3 domain of NOXO1 is four residues shorter than that of p47^{phox} (Figure 1B).

Protein structural integrity was verified for wild-type and mutant proteins (full-length and C-terminally truncated) using NMR and CD spectroscopy. There is no evidence of global or domain unfolding in any of the constructs used in this study (Figure 2 and Figure 1 of the Supporting Information). These data demonstrate that the individual domains in the linker region mutant proteins remained properly folded.

The PX−SH3$_A$ Linker Region Regulates PI(3,4)P$_2$ Binding by the PX Domain. We compared the PI(3,4)P_2 binding behavior of mutants using the liposome binding assay. Figure 3A shows typical results of binding to 0 (control) or 20% PI(3,4)P_2-containing liposomes by C-terminally truncated (1−340) or full-length (1−390) p47^{phox} in its wild-type and linker region mutant forms. The stained gels were subjected to densitometric analysis to estimate the percentage of p47^{phox} unbound (in supernatant, S) or bound (in pellet, P) to liposomes. The C-terminally truncated form of p47^{phox} has been used in our laboratories because it is somewhat more stable than the full-length form when expressed as a recombinant protein and, being shorter, yields more easily interpreted NMR spectra. The C-terminal PRR region of p47^{phox} does not affect binding to p22^{phox} (*12, 18*) or to PI(3,4)P_2 (vide infra).

Figure 3B summarizes the densitometric analysis of PI(3,4)P_2 binding by the constructs used in this study. The level of binding by any protein construct tested to 0% PI(3,4)P_2 was ~5%. The PX domain (residues 2−133) has a maximal level of binding of ~16%, close to other published data (*14*). The wild-type (full-length or truncated) protein has a binding level of ~15%. Within error, neither deletion of residues 143−150 nor mutation of residues 143−150 to glycine affects PI(3,4)P_2 binding. In marked contrast, either deletion of residues 151−158 or mutation of these residues to glycine greatly enhances PI(3,4)P_2 binding (>2-fold increase compared with that of the wild type) for both full-length and C-terminally truncated p47^{phox}. Notably, the liposome binding behavior for any particular construct (wild-type, glycine mutation, or deletion) did not differ between the full-length and C-terminally truncated form of p47^{phox}. This confirms that the C-terminal PRR (residues 341−390) does not affect PI(3,4)P_2 binding and validates comparison of the NMR analysis of p47^{phox}(1−340) with binding and activity analyses of the full-length protein. To further identify residues that affect PI(3,4)P_2 binding in the region from residue 151 to 158, we mutated residues 151−153 and residues 155−158 to glycines separately. Both mutants enhanced PI(3,4)P_2 binding when compared with that of the wild-type protein, but to a somewhat lesser extent than glycine mutation of residues 151−158. Therefore, we used glycine mutant X(151−158)G in further studies to investigate the effect of glycine mutation.

To obtain a more quantitative characterization of PI(3,4)P_2 binding, we employed SPR to investigate the PI(3,4)P_2 binding behaviors of wild-type, mutant p47^{phox}, and the isolated PX domain. Two glycine mutants of p47^{phox}(1−390), i.e., X(143−150)G and X(151−158)G, were selected because of their significant differences in PI(3,4)P_2 interaction using the liposome binding assay. Binding affinity and kinetic properties of those mutants toward PI(3,4)P_2 are summarized in Table 1.

Equilibrium binding measurements show that both wild-type and X(143−150)G p47^{phox} have very low affinities for PI(3,4)P_2. In contrast, both the isolated PX domain and the X(151−158)G mutant have substantially higher affinities for PI(3,4)P_2 (K_d = 59 and 34 μM, respectively). Under kinetic binding conditions, the X(151−158)G mutant displayed an association rate similar to that of the isolated PX domain construct. The association rates for the isolated PX domain and wild-type full-length p47^{phox} agree with published results (*14*). Notably, the dissociation behaviors of the isolated PX domain and the X(151−158)G mutant differ from each other considerably. Figure 4 shows reference-subtracted sensorgrams of PI(3,4)P_2 binding for the isolated PX domain, wild-type p47^{phox}, and the X(143−150)G and X(151−158)G mutants. The sensorgrams for the isolated PX domain, wild-type p47^{phox}, and the X(143−150G) mutant fit well with a 1:1 binding model. In contrast, the X(151−158)G mutant has markedly different dissociation behavior and is not described by a single-exponential decay. We have instead fit the dissociation stage of the X(151−158)G mutant as a biexponential decay. The first stage dissociation rate k_{d1} was 1.1 s^{-1}, similar to that of the isolated PX domain (2.5 s^{-1}). The second-stage dissociation rate was estimated to be 0.012 s^{-1}, much slower than that of the first stage. The ratio of the relative fitted amplitudes of the first and second stages was 85:15. Once again, the X(143−150)G mutant has kinetic properties similar to those of wild-type protein: both of them have an ~10-fold slower association rate when compared with the isolated PX domain and the X(151−158)G mutant. However, their dissociation rates are fairly fast, comparable to that of the isolated PX domain and k_{d1} of X(151−158)G. We note that the calculated dissociation rates for the isolated PX domain and the full-length wild type and X(143−150)G mutant exceed the range of accurate determination of the Biacore T100 instrument (suggested maximum quantifiable off rate ~ 0.5 s^{-1}, according to Biacore specifications). This fast dissociation rate may be related to the relatively weak binding of PI(3,4)P_2 liposomes by the isolated PX domain that was observed in the centrifugation-based liposome binding assay.

All the data demonstrate that (1) residues 151−158 in the linker region play a role in inhibiting the interaction of the PX domain with PI(3,4)P_2 and (2) deletion or replacement with glycines of residues 151−158 releases this inhibition and allows the PX domain to bind to PI(3,4)P_2.

NMR Relaxation Measurements Confirm That Linker Region Mutants Abolish the PX−SH3 Interaction. SPR measurement indicated that X(151−158)G behaved like the isolated PX domain with respect to both PI(3,4)P_2 binding affinity and kinetics. We further investigated the relationship between the PX domain and the remainder of X(151−158)G p47^{phox}(1−340) mutants. As evidenced from liposome binding assay results, the presence of the PRR region does not change the impact of the X(151−158)G mutations on PI(3,4)P_2 binding. Consequently, our interpretation of the

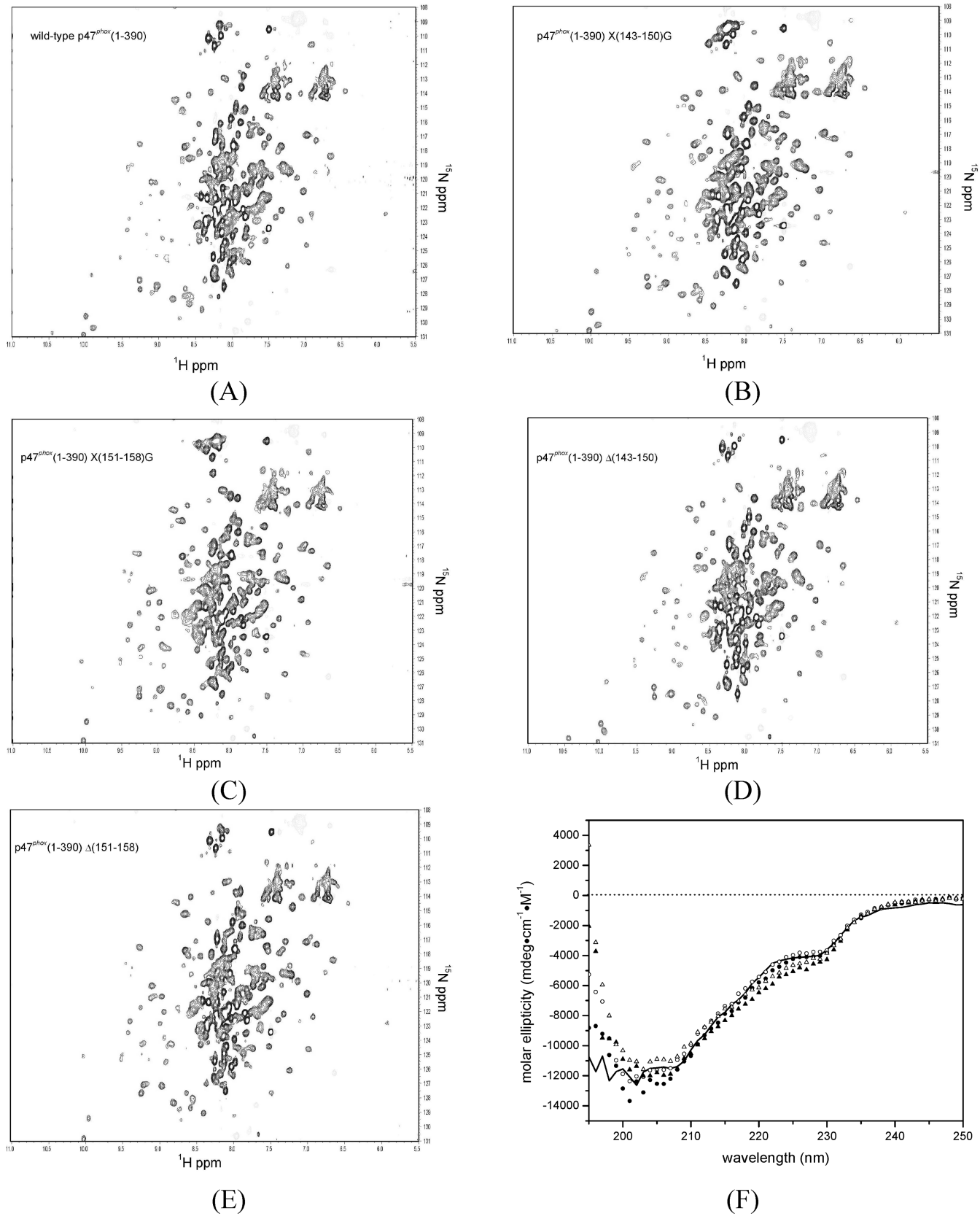

FIGURE 2: NMR and CD studies verify wild-type and mutant p47*phox* are properly folded. $^{1}H-^{15}N$ HSQC spectra for the wild type (A) and linker mutants (B−E) of p47*phox*(1−390) are very similar and show no evidence of domain unfolding as a consequence of mutation. (F) CD spectra likewise show no evidence of a change in secondary structure: (—) wild type, (●) Δ(143−150), (○) X(143−150)G, (▲) Δ(151−158), and (△) X(151−158)G. These data show that the mutations and/or deletions do not cause unfolding of the individual domains of p47*phox*. Analogous data for p47*phox*(1−340) are presented in Figure 1 of the Supporting Information.

NMR analyses of p47*phox*(1−340) is likely applicable to the full-length protein.

R_1 relaxation rates are excellent sensors of macromolecular rotational tumbling rates. We have measured backbone ^{15}N

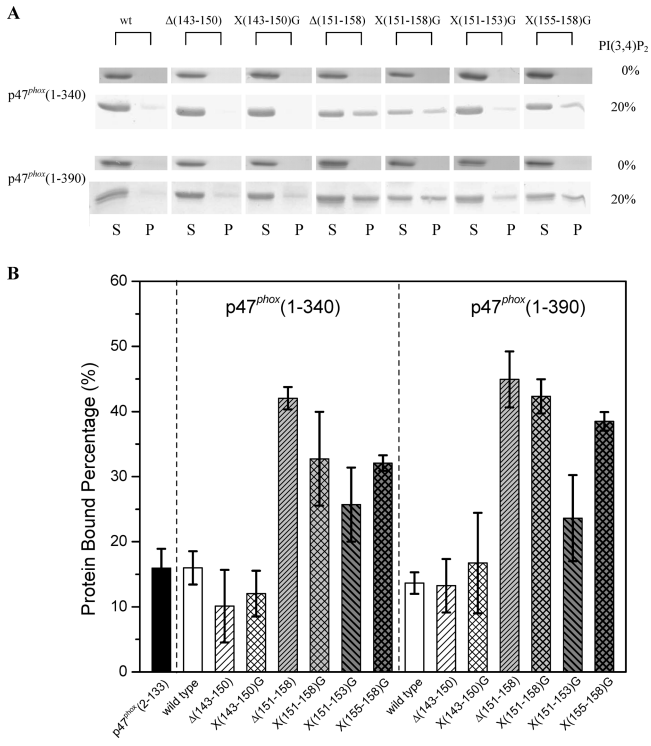

FIGURE 3: Liposome binding assays for mutants in the linker region between the PX and $SH3_A$ domains in both p47^{phox}(1−340) and p47^{phox}(1−390) show that mutations of residues 151−158 in the linker region, but not 143−150, release the PX domain for the autoinhibited state. (A) Typical stained gels from liposome binding assays showing bound protein in the liposome pellet (P) and unbound protein in the supernatant (S) for 0% (rows 1 and 3) and 20% PI(3,4)P_2 (rows 2 and 4) liposomes for p47^{phox}(1−340) and p47^{phox}(1−390). (B) Pooled binding data for 20% PI(3,4)P_2 liposomes from three independent measurements. The data represent the means ± the standard deviation. In comparison, the typical level of binding by any construct to 0% PI(3,4)P_2-containing liposomes was ∼5%.

R_1 relaxation rates for wild-type and mutant forms for p47^{phox}(1−340). Figure 5 shows a histogram of the R_1 distribution for 311 wild-type, 315 X(143−150G), and 302 X(151−158)G backbone ^{15}N atoms. The distribution of R_1 values for the wild-type protein and the X(143−150)G mutant protein exhibited a maximum at the 0.65 s^{-1} bin, while the R_1 distribution for the X(151−158)G mutant had a maximum at 0.85 s^{-1}. An R_1 of 0.65 s^{-1} is consistent with the rotational correlation time calculated for a globular 40 kDa protein (∼20 ns). The increase in R_1 observed in the X(151−158)G mutant protein suggests a reduced rotational correlation time (∼16 ns). Because the wild-type and X(151−158)G proteins have similar molecular weights, the observed increase in R_1 suggests that the X(151−158)G mutant protein is not tumbling as a single globular domain, but that instead some of the domains (most likely the PX domain and the SH3/PBR) are tumbling independently. In contrast, the R_1 distribution for the X(143−150)G mutant closely resembles that of the wild-type protein, suggesting that the X(143−150)G mutation does not disrupt the closed structure of p47^{phox}.

Sedimentation Velocity Analysis Identifies a Conformational Change in the X(151−158)G but Not the X(143−150)G Mutant. As an experimentally independent means of monitoring changes in the global conformation of p47^{phox}, we performed sedimentation velocity analyses of wild-type, X(143−150)G, and X(151−158)G p47^{phox} (both full-length and C-terminally truncated forms). We observe a small (∼1.5%) but consistent and reproducible decrease in the sedimentation coefficient, *S*, for the X(151−158)G mutant versus the wild type but no discernible shift in *S* for the X(143−150)G mutant versus the wild-type protein (Table 2).

These data are consistent with the NMR relaxation experiments that suggest global conformational rearrangement of p47^{phox} as a result of the X(151−158)G mutation to the PX−SH3 linker. That the X(151−158)G mutant sediments more slowly than either the wild type or the X(143−150)G mutant is consistent with this mutation causing dissociation of the PX domain from the autoinhibited, globular conformation to a more extended conformation.

Notably, the full-length proteins sediment more slowly than one would expect for a spherical protein with a comparable molecular weight. The experimentally determined sedimentation coefficients are ∼25% smaller than one would expect for a spherical, hydrated protein. These observations are consistent with the elongated conformation for full-length p47^{phox} reported by Durand et al. (*17*) based on SAXS data.

X(151−158)G Substantially Reduces the Level of NADPH Oxidase Activation. To determine whether the mutant p47^{phox} proteins could support NADPH oxidase activity in a system devoid of intracellular signaling events, we tested them in a cell-free system that requires lipid activators. Given that the X(151−158)G mutant protein already has a higher affinity than wild-type p47^{phox} for PI(3,4)P_2, which is a lipid activator in this system, we might expect increased oxidase activity in the presence of the X(151−158)G mutant relative to wild-type p47^{phox}. Surprisingly, both the X(143−150)G and X(151−158)G mutants supported significantly less NADPH oxidase activity than the wild-type protein in the presence of the lipid activators (Figure 6). The X(151−158)G mutation, although exhibiting clearly enhanced PI(3,4)P_2 binding activity (Figure 2), supported nearly 10-fold less NADPH oxidase activity than wild-type p47^{phox}. The X(143−150)G mutant, in contrast, leads to a retention of more than 80% wild-type NADPH oxidase activity even without a released PX domain. These data suggest that the linker region, especially residues 151−158, plays a role during the lipid-induced NADPH oxidase activation process.

DISCUSSION

The PX domain in p47^{phox} is reported to be required for the activation of NADPH oxidase and plays a role in signal transduction (*10, 16, 19, 50*). Although the interdomain interaction in p47^{phox} has been studied extensively (*9, 14, 15, 51*), it is not clear how the PX domain interacts with the remainder of the p47^{phox} molecule. Our results demonstrate that the linker region between the PX and $SH3_A$ domains helps to maintain a conformation in which the PX domain is prevented from binding PI(3,4)P_2. Mutation or deletion of the linker region does not disrupt the conformations of the individual p47^{phox} domains as shown by few changes compared with the wild-type protein in both NMR and CD spectra (Figure 2). The liposome binding assay (Figure 3) demonstrates that both glycine mutation and deletion of residues 151−158 lead to enhanced PI(3,4)P_2 binding.

Table 1: Kinetic and Affinity Measurements for p47^{phox} Proteins with Respect to PI(3,4)P_2 Measured with SPR[a]

protein	K_d from affinity measurement (μM)	k_a (M^{-1} s^{-1})	k_d (s^{-1})
p47^{phox}(2−133)	59 ± 11	47800 ± 1300	2.5 ± 0.1
wild-type p47^{phox}(1−390)	weak[b]	3200 ± 400	2.0 ± 0.1
X(143−150)G p47^{phox}(1−390)	weak[b]	2480 ± 800	1.4 ± 0.1
X(151−158)G p47^{phox}(1−390)[c]	34 ± 2	17600 ± 1900	k_{d1}, 1.1 ± 0.1; k_{d2}, 0.012 ± 0.002

[a] Data were acquired on a Biacore T100 instrument using an S series L1 sensor chip. The affinity experiments were performed at a flow rate of 5 μL/min, while kinetic data were acquired at a flow rate of 30 μL/min. The flow rate in kinetic studies was set in such a way that there was no mass transfer effect observed. The data represent the means ± the standard deviation from three independent experiments. [b] The K_d values of wild-type p47^{phox}(1−390) and X(143−150)G p47^{phox}(1−390) were beyond accurate characterization from our equilibrium data. [c] The X(151−158)G p47^{phox}(1−390) dissociation stage was modeled and fit as a two-exponential decay using Sigmaplot.

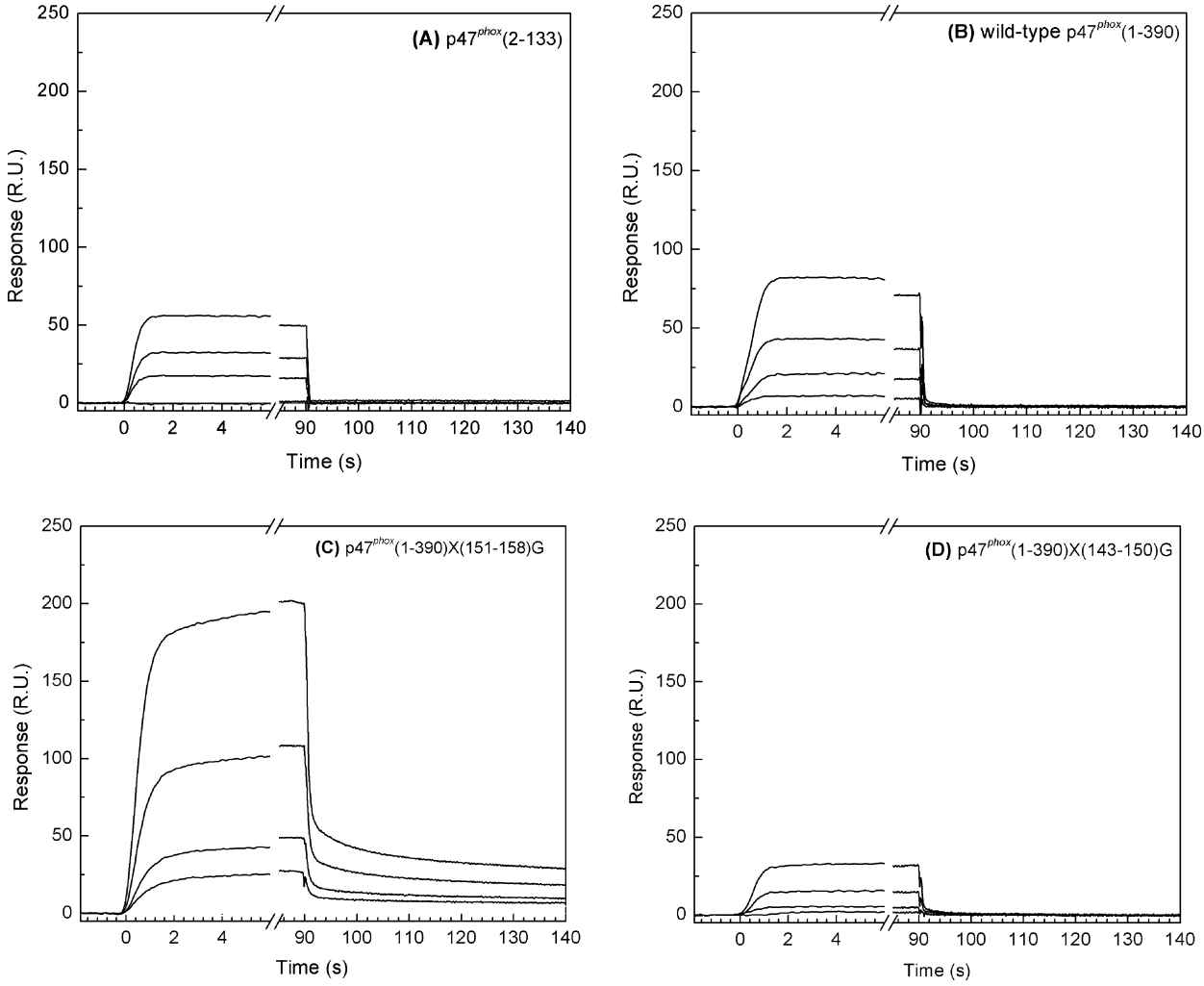

FIGURE 4: Representative kinetic binding SPR sensorgrams of measurement for p47^{phox} proteins binding to PI(3,4)P_2: (A) p47^{phox} PX domain (residues 2−133), (B) wild-type p47^{phox}(1−390), (C) X(151−158)G p47^{phox}(1−390), and (D) X(143−150)G p47^{phox}(1−390). Protein concentrations were 20, 10, 5, and 2 μM from top to bottom, respectively. The time axis has been broken to allow visualization of the rapid on rate.

SPR results (Table 1 and Figure 4) are consistent with the liposome binding assay results. The X(151−158)G mutant exhibited a PI(3,4)P_2 binding affinity and association kinetics similar to those of the isolated PX domain. However, we observed a difference in dissociation kinetics between the isolated PX domain and the X(151−158)G mutant. If we calculate the K_d of the X(151−158)G mutant using estimated second-stage dissociation rate k_{d2} and association rate k_a, the result shows a much higher affinity ($K_d \sim 7 \times 10^{-7}$ M). This K_d value agrees with previously published values of proteins with a freed PX domain (*14*). The existence of two dissociation stages suggests a possible conformation change after PX binding to PI(3,4)P_2. The isolated PX domain has a moderate affinity ($K_d = 59$ μM) and fast association and dissociation rates for PI(3,4)P_2 binding. Therefore, in the X(151−158)G mutant, a decreased dissociation rate (thus increased affinity) may indicate that other domains in p47^{phox} contribute to lipid binding. This agrees with the observation in which a freed PX domain in the p47^{phox} W263R mutant rendered a binding affinity for PI(3,4)P_2 higher than that for the isolated PX domain (*14*).

NMR relaxation analysis of the X(151−158)G mutant also provides evidence of disruption of the autoinhibited conformation (Figure 5). The increase in ^{15}N R_1 for the X(151−158)G mutant relative to the wild-type protein indicates a decrease in rotational correlation time, i.e., faster tumbling. This is consistent with the X(151−158)G mutant existing in an open form and behaving as two independently tumbling domains

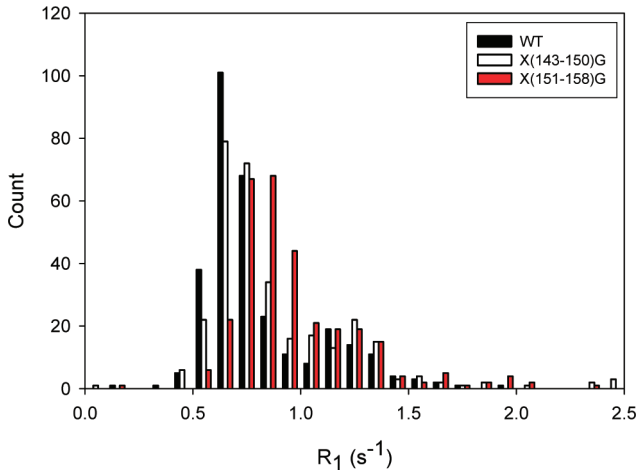

FIGURE 5: Histograms of ^{15}N spin lattice relaxation rates (R_1) showing a change in the R_1 distribution as a result of mutation of residues 151−158. Spin lattice (R_1) relaxation rates were measured for 311 (wild-type), 315 [X(143−150)G], and 302 [X(151−158)G] backbone ^{15}N atoms in p47^{phox}(1−340). The histogram bin size is 0.1 s^{-1}. The maximally populated bins are centered at 0.65 s^{-1} for the wild-type protein, 0.65 s^{-1} for X(143−150)G, and 0.85 s^{-1} for X(151−158)G.

Table 2: Sedimentation Velocity Analysis of Wild-Type and Mutant p47^{phox}[a]

	wild type	X(143−150)G	X(151−158)G
p47^{phox}(1−340)[b]	3.21 (0.09)	3.17 (0.07)	3.13 (0.05)
p47^{phox}(1−340)[c]	3.16 (0.05)	3.16 (0.06)	3.11 (0.06)
p47^{phox}(1−390)[b]	3.22 (0.01)	3.17 (0.05)	3.15 (0.06)
p47^{phox}(1−390)[c]	3.17 (0.03)	3.14 (0.05)	3.10 (0.07)

[a] $S_{20,w}$ (standard deviation from three experiments). [b] $S_{20,w}$ calculated using the SVEDBERG algorithm using the single-ideal species model. [c] $S_{20,w}$ calculated using the DCDT+ algorithm using four sets of sequential 10-scan segments.

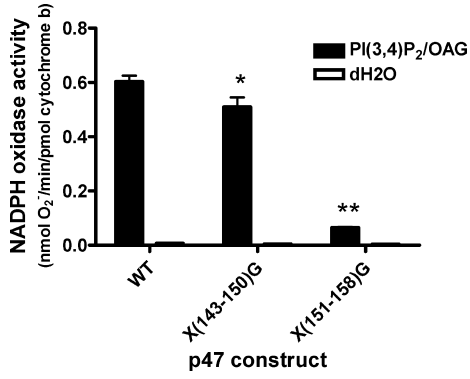

FIGURE 6: p47^{phox} linker region mutations decrease PI(3,4)P_2- and OAG-activated NADPH oxidase activity. Reaction mixtures contained either wild-type (WT) or mutant p47^{phox} recombinant proteins. PI(3,4)P_2- and OAG-activated NADPH oxidase activity was measured as described in Experimental Procedures. The data are means ± the standard error of the mean for triplicate determinations from two experiments. The NADPH oxidase activity supported by mutant p47^{phox} proteins was significantly lower than that of WT p47^{phox} where indicated (two-tailed *t* test; *$p < 0.05$; **$p < 10^{-9}$).

(PX and tandem SH3s/PBR/AIR, each ∼15 kDa), while the wild-type and X(143−150)G proteins maintain the closed state and behave as a single globular domain of ∼40 kDa. Data from liposome binding assays, SPR analyses, sedimentation velocity studies, and NMR studies all suggest that the X(151−158)G mutation, but not the X(143−150)G mutation, releases the PX domain from its autoinhibited conformation.

We observed considerable differences for isolated PX domain binding affinity between ours and those published previously (*14*). This could be a result of slightly different experimental conditions and/or equipment used in these studies. In our experiments, the salt concentration was increased to 150 mM NaCl from the value of 100 mM NaCl used in ref *14* to reduce nonspecific adsorption of proteins. The elevated salt concentration reduced the level of binding of the isolated PX domain to PI(3,4)P_2 as observed in SPR experiments (data not shown). PI(3,4)P_2 preparations from multiple sources (Cell Signals and Cayman) did not differ with respect to the PX domain affinity (data not shown). We noticed that in prior studies there is an approximately ∼100-fold decrease in affinity measured for liposomes containing 0.5% PI(3,4)P_2 compared to liposomes containing 3% PI(3,4)P_2 (*14*). Quantification of PI(3,4)P_2 at the levels required for SPR studies is difficult, and it is possible that the PI(3,4)P_2 concentration in our experiments might be different from that used in other studies even with the same nominal PI(3,4)P_2 concentration, contributing to the substantial difference in the SPR measurement.

It was expected that the X(151−158)G mutant would lead to higher NADPH oxidase activity than wild-type p47^{phox} since the X(151−158)G mutation releases the PX domain to bind with PI(3,4)P_2. However, the substantially lower observed NADPH oxidase activity (∼10% of that of the wild type) of the X(151−158)G mutant suggests that residues 151−158 play a critical role in NADPH oxidase activation.

One possible explanation is that the linker region (residues 151−158) imposes a structural organization of the PX domain relative to the SH3 domains in the membrane- and p22^{phox}-bound activated state and that mutation of these residues to glycine disrupts this structural organization. Loss of structural organization might lead to an inability of NADPH oxidase to properly assemble, resulting in decreased NADPH oxidase activity. In contrast to the X(151−158)G mutant, the X(143−150)G mutant, in which eight amino acids were also changed into glycines, has retained more than 80% of the oxidase activity of wild-type p47^{phox} (Figure 6). It was suggested that residues 151−155 are necessary for binding of p47^{phox} to p22^{phox} during activation of NADPH oxidases (*21, 22*). However, more recent studies (*12*) have shown that the tandem SH3 domains (residues 156−284) bind strongly to the p22^{phox} C-terminal tail, and the crystal structure of p47^{phox}(156−340) does not suggest a mechanism by which residues 151−155 would influence binding to p22^{phox}. These discrepancies may result from the specific constructs used in each study. The 156−340 construct used by Groemping et al. (*12*) also included eight N-terminal residues (GPLGSPEF) from the expression vector, while that used by de Mendez et al. (*21*) did not have an N-terminal extension, suggesting that the presence of several residues prior to position 156 may be required for $SH3_A$ stability, but not explicitly for p22^{phox} binding. Likewise, the presence of a GST dimer juxtaposed immediately N-terminal to $SH3_A$ may explain the requirement for spacer residues as observed by de Mendez et al. (*22*).

We subjected the protein sequence between the PX and $SH3_A$ domain (residues 122−158) to a secondary structure predicition program (*52*). The simulation predicted that the region of residues 151−158 contained a possible β sheet structure. Substituting residues from position 151 to 158 with

glycines should destroy this possible secondary structure. Kuriyan and co-workers reported that the linker region between the SH2 and SH3 domains of Src-family tyrosine kinases could form a rigid structural feature and serve as a snap-lock that clamps these two domains together (*23*). A similar mechanism could explain the role of the PX−$SH3_A$ linker in regulating the intramolecular interaction between the PX domain and the remainder of wild-type $p47^{phox}$.

On the basis of the data presented here, we propose that the PX domain and the remainder of $p47^{phox}$ are "snapped" together by a structured feature located between residues 151 and 158 to maintain the autoinhibited conformation. Elimination of this structural feature either by deletion of residues 151−158 or by mutation of these residues in this region to glycines releases the PX and allows for PI(3,4)P_2 binding. This hypothesis might also explain the constitutive phosphatidylinositol binding ability of NOXO1 (*49*). Previously, this constitutive binding property of NOXO1 was attributed to the lack of a PBR/AIR counterpart in NOXO1 (*17*). Examination of the protein sequences of $p47^{phox}$ and NOXO1 shows that NOXO1 lacks residues corresponding to residues 155−158 of $p47^{phox}$ (Figure 1B) (*48*). The absence of a snap-lock between the PX and SH3 domains of NOXO1 could be related to the constitutive binding of NOXO1 to membranes.

To summarize, we have employed multiple, complementary techniques to investigate the structural and functional role of the linker region between the PX and $SH3_A$ domains, specifically residues 143−158, in $p47^{phox}$. Our liposome binding assay results and SPR measurements confirm that residues 151−158 play a role in regulating binding of the PX domain to PI(3,4)P_2, while residues 143−150 do not play such a role. Glycine mutation of residues 151−158 releases the PX domain from an autoinhibitory interaction(s), and this allows PI(3,4)P_2 binding. NMR relaxation data from $p47^{phox}$(1−340) and sedimentation velocity data from both $p47^{phox}$(1−340) and $p47^{phox}$(1−390) constructs also support dissociation of the PX domain from the remainder of the molecule in the X(151−158)G mutant. The removal or mutation to glycine of residues 151−158 leads to a reduction of the NADPH oxidase activation level, possibly through a loss of a structural feature that restricts the orientations of the PX and SH3 domains. Full activation of NADPH oxidase likely requires that the PX and SH3 domains interact with other NADPH oxidase subunits such as $p67^{phox}$ and $p22^{phox}$. Our data suggest that intramolecular communication in $p47^{phox}$ is more complex than previously suggested (*12, 14, 17, 18*). This study, however, does not directly investigate the structure of the fully autoinhibited form of $p47^{phox}$ and thus does not allow us to confirm or refute either of the aforementioned models for inhibition of PX−lipid binding. Further direct structural information about the relative domain positions in $p47^{phox}$ is required to understand the autoinhibitory mechanism(s) in $p47^{phox}$.

ACKNOWLEDGMENT

We thank Mary C. Stahle and Nicole Y. Davis for their assistance in SPR experiments. Joel V. Tuttle helped to prepare the X(151−158)G $p47^{phox}$(1−390) mutant.

SUPPORTING INFORMATION AVAILABLE

Characterization of the folding state of wild-type and mutant $p47^{phox}$(1−340) by NMR and CD. This material is available free of charge via the Internet at http://pubs.acs.org.

REFERENCES

1. Nathan, C. (2006) Neutrophils and immunity: Challenges and opportunities. *Nat. Rev. Immunol. 6*, 173–182.
2. Babior, B. M. (2004) NADPH oxidase. *Curr. Opin. Immunol. 16*, 42–47.
3. Quinn, M. T., Ammons, M. C. B., and Deleo, F. R. (2006) The expanding role of NADPH oxidases in health and disease: No longer just agents of death and destruction. *Clin. Sci. 111*, 1–20.
4. Heyworth, P. G., Cross, A. R., and Curnutte, J. T. (2003) Chronic granulomatous disease. *Curr. Opin. Immunol. 15*, 578–584.
5. Finkel, T. (2000) Redox-dependent signal transduction. *FEBS Lett. 476*, 52–54.
6. DeLeo, F. R., and Quinn, M. T. (1996) Assembly of the phagocyte NADPH oxidase: Molecular interaction of oxidase proteins. *J. Leukocyte Biol. 60*, 677–691.
7. Babior, B. M., Lambeth, J. D., and Nauseef, W. (2002) The neutrophil NADPH oxidase. *Arch. Biochem. Biophys. 397*, 342–344.
8. Heyworth, P. G., Curnutte, J. T., Nauseef, W. M., Volpp, B. D., Pearson, D. W., Rosen, H., and Clark, R. A. (1991) Neutrophil nicotinamide adenine dinucleotide phosphate oxidase assembly. Translocation of p47-phox and p67-phox requires interaction between p47-phox and cytochrome b558. *J. Clin. Invest. 87*, 352–356.
9. Groemping, Y., and Rittinger, K. (2005) Activation and assembly of the NADPH oxidase: A structural perspective. *Biochem. J. 386*, 401–416.
10. Kanai, F., Liu, H., Field, S. J., Akbary, H., Matsuo, T., Brown, G. E., Cantley, L. C., and Yaffe, M. B. (2001) The PX domains of p47phox and p40phox bind to lipid products of Pl(3)K. *Nat. Cell Biol. 3*, 675–678.
11. Stephens, L., Ellson, C., and Hawkins, P. (2002) Roles of PI3Ks in leukocyte chemotaxis and phagocytosis. *Curr. Opin. Cell Biol. 14*, 203–213.
12. Groemping, Y., Lapouge, K., Smerdon, S. J., and Rittinger, K. (2003) Molecular basis of phosphorylation-induced activation of the NADPH oxidase. *Cell 113*, 343–355.
13. Yuzawa, S., Ogura, K., Horiuchi, M., Suzuki, N. N., Fujioka, Y., Kataoka, M., Sumimoto, H., and Inagaki, F. (2004) Solution structure of the tandem src homology 3 domains of p47phox in an autoinhibited form. *J. Biol. Chem. 279*, 29752–29760.
14. Karathanassis, D., Stahelin, R. V., Bravo, J., Perisic, O., Pacold, C. M., Cho, W. W., and Williams, R. L. (2002) Binding of the PX domain of p47phox to phosphatidylinositol 3,4-bisphosphate and phosphatidic acid is masked by an intramolecular interaction. *EMBO J. 21*, 5057–5068.
15. Hiroaki, H., Ago, T., Ito, T., Sumimoto, H., and Kohda, D. (2001) Solution structure of the PX domain, a target of the SH3 domain. *Nat. Struct. Biol. 8*, 526–530.
16. Ago, T., Kuribayashi, F., Hiroaki, H., Takeya, R., Ito, T., Kohda, D., and Sumimoto, H. (2003) Phosphorylation of p47phox directs phox homology domain from SH3 domain toward phosphoinositides, leading to phagocyte NADPH oxidase activation. *Proc. Natl. Acad. Sci. U.S.A. 100*, 4474–4479.
17. Durand, D., Cannella, D., Dubosclard, V., Pebay-Peyroula, E., Vachette, P., and Fieschi, F. (2006) Small-angle X-ray scattering reveals an extended organization for the autoinhibitory resting state of the $p47^{phox}$ modular protein. *Biochemistry 45*, 7185–7193.
18. Yuzawa, S., Suzuki, N. N., Fujioka, Y., Ogura, K., Sumimoto, H., and Inagaki, F. (2004) A molecular mechanism for autoinhibition of the tandem SH3 domains of $p47^{phox}$, the regulatory subunit of the phagocyte NADPH oxidase. *Genes Cells 9*, 443–456.
19. Ago, T., Takeya, R., Hiroaki, H., Kuribayashi, F., Ito, T., Kohda, D., and Sumimoto, H. (2001) The PX domain as a novel phosphoinositide-binding module. *Biochem. Biophys. Res. Commun. 287*, 733–738.
20. Ellson, C., Davidson, K., Anderson, K., Stephens, L. R., and Hawkins, P. T. (2006) PtdIns3P binding to the PX domain of p40phox is a physiological signal in NADPH oxidase activation. *EMBO J. 25*, 4468–4478.

21. de Mendez, I., Adams, A. G., Sokolic, R. A., Malech, H. L., and Leto, T. L. (1996) Multiple SH3 domain interactions regulate NADPH oxidase assembly in whole cells. *EMBO J. 15*, 1211–1220.
22. de Mendez, I., Homayounpour, N., and Leto, T. L. (1997) Specificity of p47phox SH3 domain interactions in NADPH oxidase assembly and activation. *Mol. Cell. Biol. 17*, 2177–2185.
23. Young, M. A., Gonfloni, S., Superti-Furga, G., Roux, B., and Kuriyan, J. (2001) Dynamic coupling between the SH2 and SH3 domains of c-Src and Hck underlies their inactivation by C-terminal tyrosine phosphorylation. *Cell 105*, 115–126.
24. Tortorella, D., Ulbrandt, N. D., and London, E. (1993) Simple centrifugation method for efficient pelleting of both small and large unilamellar vesicles that allows convenient measurement of protein binding. *Biochemistry 32*, 9181–9188.
25. Lehman, N., Ledford, B., Di Fulvio, M., Frondorf, K., McPhail, L. C., and Gomez-Cambronero, J. (2007) Phospholipase D2-derived phosphatidic acid binds to and activates ribosomal p70 S6 kinase independently of mTOR. *FASEB J. 21*, 1075–1087.
26. Candiano, G., Bruschi, M., Musante, L., Santucci, L., Ghiggeri, G. M., Carnemolla, B., Orecchia, P., Zardi, L., and Righetti, P. G. (2004) Blue silver: A very sensitive colloidal Coomassie G-250 staining for proteome analysis. *Electrophoresis 25*, 1327–1333.
27. Stahelin, R. V., Karathanassis, D., Murray, D., Williams, R. L., and Cho, W. (2007) Structural and membrane binding analysis of the phox homology domain of bem1p: Basis of phosphatidylinositol 4-phosphate specificity. *J. Biol. Chem. 282*, 25737–25747.
28. Erb, E. M., Chen, X. Y., Allen, S., Roberts, C. J., Tendler, S. J. B., Davies, M. C., and Forsen, S. (2000) Characterization of the surfaces generated by liposome binding to the modified dextran matrix of a surface plasmon resonance sensor chip. *Anal. Biochem. 280*, 29–35.
29. Narayan, K., and Lemmon, M. A. (2006) Determining selectivity of phosphoinositide-binding domains. *Methods 39*, 122–133.
30. Manna, D., Albanese, A., Park, W. S., and Cho, W. (2007) Mechanistic Basis of Differential Cellular Responses of Phosphatidylinositol 3,4-Bisphosphate- and Phosphatidylinositol 3,4,5-Trisphosphate-binding Pleckstrin Homology Domains. *J. Biol. Chem. 282*, 32093–32105.
31. Pervushin, K., Riek, R., Wider, G., and Wuthrich, K. (1997) Attenuated T_2 relaxation by mutual cancellation of dipole-dipole coupling and chemical shift anisotropy indicates an avenue to NMR structures of very large biological macromolecules in solution. *Proc. Natl. Acad. Sci. U.S.A. 94*, 12366–12371.
32. Yang, D. W., and Kay, L. E. (1999) Improved ^{1}HN-detected triple resonance TROSY-based experiments. *J. Biomol. NMR 13*, 3–10.
33. Nietlispach, D. (2005) Suppression of anti-TROSY lines in a sensitivity enhanced gradient selection TROSY scheme. *J. Biomol. NMR 31*, 161–166.
34. Chill, J. H., Louis, J. M., Baber, J. L., and Bax, A. (2006) Measurement of ^{15}N relaxation in the detergent-solubilized tetrameric KcsA potassium channel. *J. Biomol. NMR 36*, 123–136.
35. Delaglio, F., Grzesiek, S., Vuister, G. W., Zhu, G., Pfeifer, J., and Bax, A. (1995) NMRPipe: A multidimensional spectral processing system based on UNIX pipes. *J. Biomol. NMR 6*, 277–293.
36. Johnson, B. A., and Blevins, R. A. (1994) NMR View: A computer program for the visualization and analysis of NMR data. *J. Biomol. NMR 4*, 603–614.
37. Philo, J. S. (2000) A method for directly fitting the time derivative of sedimentation velocity data and an alternative algorithm for calculating sedimentation coefficient distribution functions. *Anal. Biochem. 279*, 151–163.
38. Philo, J. S. (2006) Improved methods for fitting sedimentation coefficient distributions derived by time-derivative techniques. *Anal. Biochem. 354*, 238–246.
39. Stafford, W. F. (1992) Boundary analysis in sedimentation transport experiments: A procedure for obtaining sedimentation coefficient distributions using the time derivative of the concentration profile. *Anal. Biochem. 203*, 295–301.
40. Laue, T. M., Shah, B. D., Ridgeway, T. M., and Pelletier, S. (1992) Computer-aided interpretation of analytical sedimentation data for proteins. In *Analytical Ultracentrifugation in Biochemistry and Polymer Science* (Harding, S. E., Rowe, A. J., and Horton, J. C., Eds.) Redwood Press, Cambridge, U.K.
41. Philo, J. S. (1997) An improved function for fitting sedimentation velocity data for low-molecular-weight solutes. *Biophys. J. 72*, 435–444.
42. Sergeant, S., and McPhail, L. C. (1997) Opsonized zymosan stimulates the redistribution of protein kinase C isoforms in human neutrophils. *J. Immunol. 159*, 2877–2885.
43. Metcalf, J. A. (1986) *Laboratory manual of neutrophil function*, Raven Press, New York.
44. Qualliotinemann, D., Agwu, D. E., Ellenburg, M. D., McCall, C. E., and McPhail, L. C. (1993) Phosphatidic acid and diacylglycerol synergize in a cell-free system for activation of the NADPH oxidase from human neutrophils. *J. Biol. Chem. 268*, 23843–23849.
45. Rouser, G., Siakotos, A., and Fleischer, S. (1966) Quantitative analysis of phospholipids by thin-layer chromatography and phosphorus analysis of spots. *Lipids 1*, 85–86.
46. Palicz, A., Foubert, T. R., Jesaitis, A. J., Marodi, L., and McPhail, L. C. (2001) Phosphatidic acid and diacylglycerol directly activate NADPH oxidase by interacting with enzyme components. *J. Biol. Chem. 276*, 3090–3097.
47. Massey, V. (1959) The microestimation of succinate and the extinction coefficient of cytochrome c. *Biochim. Biophys. Acta 34*, 255–256.
48. Cheng, G. J., and Lambeth, J. D. (2005) Alternative mRNA splice forms of NOXO1: Differential tissue expression and regulation of Nox1 and Nox3. *Gene 356*, 118–126.
49. Cheng, G. J., and Lambeth, J. D. (2004) NOXO1, regulation of lipid binding, localization, and activation of Nox1 by the phox homology (PX) domain. *J. Biol. Chem. 279*, 4737–4742.
50. Yaffe, M. B. (2002) The p47phox PX domain: Two heads are better than one. *Structure 10*, 1288–1290.
51. Nagasawa, T., Ebisu, K., Inoue, Y., Miyano, K., and Tamura, M. (2003) A new role of Pro-73 of p47phox in the activation of neutrophil NADPH oxidase. *Arch. Biochem. Biophys. 416*, 92–100.
52. Rost, B., and Liu, J. (2003) The PredictProtein server. *Nucleic Acids Res. 31*, 3300–3304.

BI8005847